Observed responses of mesospheric water vapor to solar cycle and dynamical forcings

Ellis Remsberg[1], Robert Damadeo[1], Murali Natarajan[1], and Praful Bhatt[2]

[1]Science Directorate, NASA Langley Research Center

21 Langley Blvd.

Hampton, Virginia 23681, USA

[2]Robinhood

3200 Ash Street

Palo Alto, CA 94306, USA

(corresponding author e-mail: ellis.e.remsberg@nasa.gov)

KEY POINTS

Main point #1: Analyses of time series of mesospheric H_2O from HALOE make use of the Lyman-α flux proxy as the solar flux forcing term in two separate regression model approaches.

Main point #2: Annual average H_2O has a large negative response at solar maximum in the upper mesosphere and a very weak positive response in the tropical lower mesosphere.

Main point #3: There are significant negative H_2O responses in the northern hemisphere to the ENSO index that indicate effects of wave drag for the net circulation of the mesosphere.

Abstract. This study focuses on responses of mesospheric water vapor (H_2O) to the solar cycle flux at Lyman-α wavelength and to wave forcings according to the multivariate ENSO index (MEI). The zonal-averaged responses are for latitudes from 60°S to 60°N and pressure-altitudes from 0.01 to 1.0 hPa, as obtained by multiple linear regression (MLR) analyses of time series of H_2O from the Halogen Occultation Experiment (HALOE) for July 1992 to November 2005. The solar responses change from strong negative H_2O values in the upper mesosphere to very weak, positive values in the tropical lower mesosphere. Those response profiles at the low latitudes agree reasonably with published results for H_2O from the Microwave Limb Sounder (MLS). The distribution of seasonal H_2O amplitudes corresponds well with that for temperature and is in accord with the seasonal net circulation. In general, the responses of H_2O to MEI are anti-correlated with those of temperature. H_2O responses to MEI are negative in the upper mesosphere and largest in the northern hemisphere; responses in the lower mesosphere are more symmetric with latitude. The H_2O trends from MLR for the lower mesosphere agree with those reported from time series of microwave observations at two ground-based network stations.

1. Introduction

Distributions and trends of water vapor (H_2O) and from numerical models are available as a function of altitude and latitude for the middle atmosphere [e.g., *Garcia et al.*, 2007; *Marsh et al.*, 2007; *Schmidt et al.*, 2006]. *Remsberg* [2010] reported on long-term variations of H_2O in the mesosphere observed with the Halogen Occultation Experiment (HALOE) instrument [*Russell et al.*, 1993; *Grooss and Russell*, 2005] that operated aboard the Upper Atmosphere Research Satellite (UARS), as a useful diagnostic of the performance of the radiative-chemical-transport models. Results of a similar study for the low latitudes are in *Nath et al.* [2017], based on H_2O from the Microwave Limb Sounder (MLS) of the AURA satellite. The present study is a re-analysis of the HALOE H_2O time series with the goal of quantifying its responses to dynamical and solar cycle forcings throughout the mesosphere and for comparison with results from MLS.

Figure 1 shows the annual average distribution of the H_2O mixing ratio from HALOE between 60°S and 60°N latitude and from 0.01 to 1.0 hPa, and it is representative of the time span of 1992 through 2005. The data for Fig. 1 are from the constant terms of multiple linear regression (MLR) analyses of a set of time series of HALOE H_2O at specified latitudes and pressure-altitudes. Notable features of the distribution are its maximum of ~6.6 ppmv at 7.5°S and 0.05 to 0.07 hPa plus a nearly symmetric decrease toward higher latitudes in both hemispheres. The rapid decrease of H_2O from 0.05 hPa to near the mesopause is due to photolysis by the solar flux at Lyman-α (Ly-α) wavelengths. Smaller, annual average H_2O values at higher latitudes are from the seasonal effects of a net meridional transport of the low mixing ratios in the uppermost mesosphere toward polar latitudes followed by descent in the winter hemisphere. The H_2O maximum is a result of the nearly complete oxidation of methane (CH_4) to H_2O during ascent at low latitudes of air from the upper stratosphere to the middle mesosphere, as added to the underlying H_2O entering into the tropical lower stratosphere. Mixing and dissipation of planetary and gravity waves act to reduce the gradients of H_2O within Fig. 1.

Nicolet [1981] calculated that there should be a greater loss of H_2O in the upper mesosphere at solar maximum, due to enhancements of the flux at Ly-α. Previous analyses of H_2O from

HALOE show the enhanced loss at solar maximum [*Chandra et al.*, 1997; *Randel et al.*, 2000; *Hervig and Siskind*, 2006; *Nedoluha et al.*, 2009; *Remsberg*, 2010]. Numerical model results of the response of H_2O over the solar cycle agree reasonably with those observed findings [*Garcia et al.*, 1984; *Schmidt et al.*, 2006; *Marsh et al.*, 2007]. *Remsberg* [2010] thought that the responses of H_2O to the solar cycle forcing might also experience aliasing by decadal-scale dynamical effects. Therefore, he fit an 11-yr sinusoid to the HALOE H_2O data series and checked to see if its phase was anti-correlated with the solar flux. Although a sinusoid is merely an approximation for the flux variations, he found that the decadal-scale variations of H_2O were anti-phased with solar cycle maximum in the upper mesosphere, as expected. Yet, his 11-yr H_2O maximum appeared to lag solar cycle minimum by 1-2 years in the tropical middle mesosphere. The present re-analyses make use of the more appropriate, solar Ly-α flux time series and include a term to account for modulation of upward propagating waves and their dissipating effects related to variations of the El-Nino/Southern Oscillation (ENSO) index.

Section 2 reviews characteristics of the HALOE H_2O and of the MLR model used for the re-analysis of its data time series. Section 3 reports on a hemispheric asymmetry of the annual cycle amplitudes for both H_2O and temperature, an indication of differences in the net transport in the two hemispheres. Section 4 shows significant responses in the northern hemisphere for both temperature and H_2O to the wave activity associated with ENSO. Section 5 contains the updated results of the responses of H_2O to the solar forcings and extends those findings through the lower mesosphere. Section 6 shows the associated H_2O trends and compares them with ones reported by *Nedoluha et al.* [2017] for 1992-2005 from two ground-based microwave radiometer sites. Section 7 comments on results from a separate simultaneous temporal and spatial (STS) analysis method that accounts for diurnal effects and for any biases due to changes in the sampling with latitude from HALOE. Section 8 compares the current HALOE results with those of MLS of *Nath et al.* [2017] and with the initial HALOE analyses of *Remsberg* [2010]. Section 9 summarizes the primary findings of the present study.

2. Data characteristics and analysis methods

The HALOE Version 19 (V19) H_2O data are described in *Kley et al*. [2000] and in *Gordley et al.* [2009], particularly in terms of their suitability for trend studies and for obtaining responses to the solar cycle flux. The HALOE instrument obtained measurements of atmospheric transmission through the Earth atmosphere limb via solar occultation. Its retrieved H_2O mixing ratio profiles have a vertical resolution of ~2.3 km. Individual transmission profiles are sensitive to detector noise and any tracking jitter, or small variations in the measurement scan angles. Retrieved H_2O profiles exhibit pronounced structure in the mesosphere because the transmission data are noisy and the limb absorption in the H_2O channel at 6.6 µm is due to strong, nearly saturated lines. Effects of the noise become smaller after taking averages of the retrieved sunrise (SR) or sunset (SS) H_2O profiles, as they occur across several successive days and within a latitude bin. A bin width of 15° having a minimum of five profiles yields representative zonal mean results, as gradients of H_2O within a bin tend to be small and variations at a pressure level are mainly due to random error. Most times, the SR and SS profiles occur days apart and alternate for a given 15°-wide latitude zone, according to the orbital geometry for the occultation sampling by HALOE. Those SR and SS occurrences have an average spacing of about 23 days, which is often enough for resolving the semi-annual and longer period cycles. There is no adjustment made for a systematic SR/SS difference in the H_2O data time series.

The bin-averaged HALOE H_2O is in terms of 104 individual time series for analysis, at eight latitude bins (with central latitudes of 52.5°S to 52.5°N spaced every 15°) and at thirteen pressure-altitudes (0.01 to 1.0 hPa). There are anomalies in a few of the retrieved HALOE H_2O profiles due to uncorrected "lockdown" and "trip angle" effects, the latter most notably for SR profiles in November 1991 and April 1992 and also intermittently from 2001-2003. Those anomalous profiles are not included in the present analyses; a list of them is located at the HALOE Website (*http://haloe.gats-inc.com/home/index.php/*) under the menu item "Two Problems in the Data". The instruments on UARS also did not take data from early June and into July of 1992. There are also fewer H_2O data in the lower stratosphere prior to July 1992 due to attenuation of signal for the HALOE solar tracker as it scanned across the Pinatubo aerosol layer [*Remsberg et al.*, 1996]. Accordingly, the HALOE data time series have a start time of July 1992 for the current study.

The MLR analysis modeling for H_2O mixing ratio for a given latitude bin and pressure is analogous to that of *Remsberg* [2010] and is as follows.

$$H_2O\ (t) = \alpha(t) + \beta * t + \gamma * Lya(t) + \delta * ENSO(t) + residual(t) \quad , \qquad \text{Eq. (1)}$$

where $\alpha(t) = \text{Const.} + \Sigma_{i=1,3}\ [A_i \cos \omega_i t + B_i \sin \omega_i t\ ]$, and ω_i has periods of 6, 12, and 28 months for semi-annual (SAO), annual (AO), and QBO-like cycles, respectively. The two periodic, 853 day (~28 month) terms are fit to the H_2O data at a given latitude and pressure-altitude to account for effects of the QBO-like forcings that occur more regularly in the upper stratosphere and mesosphere [*Baldwin et al.*, 2001], which differs from the more customary proxy time series of observed tropical QBO winds of the lower stratosphere. The sine and cosine functions of each periodic term have transforms to single principal angle terms, giving their amplitude and phase. The remaining terms are a Constant, a linear trend (Lin or β), a normalized, solar Ly-α flux proxy (Lya or γ), and a multivariate ENSO index or MEI proxy (ENSO or δ). No effects from the eruption of Mt. Pinatubo of June 1991 [e.g., *She et al*., 1998; *Lee and Smith*, 2003] are apparent in the H_2O model residuals; thus, no volcanic proxy term is included.

Figure 2 is an example MLR model fit to the data time series of SR and SS points at 37.5±7.5°N latitude and at 0.015 hPa. The oscillating curve is the combination of all the terms, while the straight line is the sum of just the Constant and Lin terms. Singular value decomposition (SVD) methods determine the coefficients and uncertainties for the terms of the MLR modeling, as in *Remsberg* [2010]. Most often, there is a positive memory, or lag-1 autoregressive (AR1) character for the bin-averaged time series data. That effect is accounted for following the two-step method of *Cochrane and Orcutt* [1949], as applied to geophysical data (e.g., *Tiao et al.* [1990]). That is, there is an initial fitting of the data to give MLR term coefficients assuming no memory, or AR1 = 0. Then a first-order, autocorrelation coefficient (AR1) is determined from the model minus data residuals, followed by a transformation of each MLR model term to account for that lag. AR1 = 0.10 for the data series in Fig. 2. Once the AR1 effect is considered, the analyzed amplitudes are smaller from the transformed periodic terms.

The current MLR modeling uses a solar cycle flux term based on the proxy time series of Ly-α flux having units of 10^{11} photons/cm^2/s. By definition, the Lya term is directly in-phase with solar activity, whereas the 11-yr sinusoid fit to the data of *Remsberg* [2010] is an approximation. The Ly-α flux has a smoothing over 81 days to minimize shorter-term effects from 27-dy solar rotation cycles, and those smoothed values vary between 3.6 units and 5.9 units. For comparison, the corresponding variation of the F10.7 flux proxy is 70 to 220 solar flux units (sfu). Figure 3 shows the normalized, quasi-periodic Ly-α flux values that coincide with the discrete, bin-averaged HALOE SR and SS samplings at 37.5°N from July 1992 to November 2005. Minimum values are near day 2100 (mid-1996) and maximum values are near day 4100 (early 2002). For 1991 through early 1992 the smoothed fluxes are larger or of order 6.0 (not shown in Figure 3), followed by an abrupt drop to about 4.8 by July 1992.

Figure 4 shows the Multivariate ENSO Index (MEI) that corresponds to the discrete HALOE H_2O values at 37.5°N. MEI values near day 2500 are of order 3.0 and are associated with the strong El Nino event of 1997-98. In effect, El Nino alters the stratospheric temperature and zonal wind distributions, thereby modifying the upward propagation of tropospheric wave activity to the mesosphere [*Li et al.*, 2008]. MEI values retain their magnitude and sign for the MLR modeling, and the responses of H_2O have units of % of average H_2O MEI^{-1}.

Table 1 gives the coefficients and standard deviations (σ) of all the terms of the final MLR model for the time series at 37.5±7.5°N latitude and at 0.015 hPa (Figure 2), along with confidence intervals (CI in %) indicating the likely presence of each term in the data time series. Annual cycle (AO), semi-annual cycle (SAO), Lya, ENSO, and trend (Lin) terms are highly significant in the data series. Only the QBO-like term has little significance. Maximum values occur in mid-summer at this latitude. The H_2O response to Ly-α forcing is anti-phased, and the response to the ENSO term is negative. The coefficient of the linear trend term is positive or increasing at a rate of 5.0 %/decade.

An important test for acceptance of the final MLR model is that there be no significant structure remaining in the data minus model residual series. One instance where the model of Eq (1) is deficient is for the time series at 22.7°S and 0.03 hPa. Figure 5 shows that the data points are not fit well by the model terms for the latter part of 2002. There was a large, planetary wave-1 anomaly in the mid to upper mesosphere of the southern hemisphere in September 2002, related to a rare, mid-winter stratospheric warming/mesospheric cooling event [*Palo et al.*, 2005]. Low H_2O values are also present in the time series for 0.02 and 0.05 hPa at the same latitude and season (not shown). However, the Eq. (1) does not include a proxy term for an episodic event. The climatological average contours of Figure 1 show that there are significant meridional gradients for H_2O at middle latitudes of the middle to upper mesosphere. While there must have been equatorward transport of low H_2O values to 22.7°S for 2002, this report does not analyze that event further.

3. Analyzed seasonal and interannual responses

Seasonal variations with latitude in the upper mesosphere come from the effects of the large-scale meridional circulation that is upward in the summer hemisphere and downward in the winter hemisphere. Figure 6 is the distribution of the AO amplitudes (as a percentage of the Constant term) from the MLR models. AO amplitudes are smallest at low latitudes, but with a minimum response of between 3 to 5% centered near 10°S. The corresponding distribution of semi-annual (SAO) H_2O amplitudes (not shown) is more symmetric about the Equator with minimum values in the subtropics, in accord with *Remsberg* [2010, his Figure 4]. In general, the AO and SAO terms have a CI > 95% in the upper mesosphere, and their respective amplitude distributions agree with those found by *Lossow et al.* [2008] from measurements with the submillimeter radiometer (SMR) on the ODIN satellite. The HALOE AO and SAO amplitudes are weak across 60°S to 60°N for the lower mesosphere, where climatological H_2O in Figure 1 has almost no spatial gradient and for which the effects wave activity are small.

Figure 7 is an update of the HALOE distribution of AO temperature amplitudes in *Remsberg* [2007], but based now on MLR analyses using the same set of terms and locations as for H_2O. Fig. 7 shows small values (2 to 3 K) in the tropical upper mesosphere with minimum values centered near 10°S. The AO amplitude pattern for temperature is primarily a result of seasonal radiative forcings from ozone and CO_2 and related net transport, while the pattern for H_2O confirms the role of the net seasonal circulation and the effects of wave dissipation and mixing. Further, since H_2O has a large vertical gradient in the uppermost mesosphere, its minimum AO value in Fig. 6 implies a near-zero, annual average vertical transport at the low latitudes. The results of both Figures 6 and 7 ought to be useful diagnostics of the quality of climate model simulations for the mesosphere.

The QBO-like term has amplitudes (not shown) that are of order 1 to 1.5% in the tropics; smaller values occur from the subtropics to middle latitudes. Amplitudes are largest at high latitudes of the northern hemisphere and at 7.5°N near the mesopause, although they are not significant at either location. In general, this dynamical forcing term is of minor importance for the MLR modeling of both H_2O and temperature in the mesosphere.

4. Responses of temperature and H_2O to the ENSO index

Mesospheric temperatures at high latitudes are warm in winter and cold in summer. Large-scale transport in that region occurs according to a residual mean meridional circulation having maximum values near 75 km, moving toward the winter hemisphere, and descending at the Pole (e.g., see Fig. 7.4 of *Andrews et al.* [1987]). Both planetary and gravity waves propagate to the mesosphere in the presence of zonal westerlies in the late fall and winter seasons, and wave activity is greater during the warm phase (positive MEI) of El Nino [*Li et al.*, 2016]. That wave activity dissipates in the upper mesosphere, causing a drag on or slowing of the net circulation and leading to downwelling (and warming) in the tropics and upwelling (and cooling) at middle and high latitudes [*Li et al.*, 2013; 2016].

The HALOE temperature response distribution to MEI is in Figure 8. Values are generally positive in the tropical middle mesosphere and at middle latitudes of the upper mesosphere. Responses of 0.6 to 0.8 K/Mei near 75 km at 20°N in Fig. 8 are similar to the annual-average results (~1 K/Mei) from lidar measurements at Hawaii (19°N) in *Li et al.* [2008, their Figure 7]. The changeover from 0.8 K/Mei in the tropics to -0.8 K/Mei in the extratropics at about 65 km in Fig. 8 also agrees with the pattern of observed findings, as reported by *Li et al.* [2013; 2016] from wintertime data of the Sounding of the Atmosphere using Broadband Emission Radiometry (SABER) experiment. However, Fig. 8 is an average estimate for the HALOE period, so the overall effects from Mei are for both southern and northern hemisphere winters. The somewhat larger negative responses at 0.1 hPa and NH middle latitudes implies greater wintertime wave activity in that region, most likely related to midwinter stratospheric warming events.

H_2O is a tracer molecule for the mesosphere, and its observed responses to MEI should indicate the effects of wave activity on the net circulation, too. Figure 9 displays the responses of H_2O (as percentages of the climatological values in Fig. 1) to the MEI index for mid-1992 through 2005. Those responses are most negative (for positive MEI) in the upper mesosphere of the northern hemisphere, particularly in the subtropics. This region is where the wave dissipation exerts a drag on the net circulation and slows the transport of higher H_2O mixing ratios from the summer to the winter hemisphere. Weaker negative responses occur at southern hemisphere latitudes across the rather narrow pressure range of 0.04 to 0.02 hPa. The results in Figs. 8 and 9 show that the responses of H_2O are anti-correlated with those of temperature and are due, presumably, to corresponding anomalies for the residual meridional circulation. The responses of temperature to MEI display good hemispheric symmetry and indicate the effects of waves on the larger-scale diabatic circulation. The responses of H_2O in the upper mesosphere are not symmetric but are clearly larger and more significant for the northern hemisphere. Conversely, the responses are smaller, more symmetric, yet still significant at middle latitudes of the lower mesosphere.

Figure 10 presents climatological H_2O distributions from HALOE based on their Constant, AO, and SAO terms for mid-January (at top for day 15) and for mid-July (at bottom for day 198). The two panels show the large H_2O differences at solstice with lowest values in the upper mesosphere in winter. *Schmidt et al.* [2006] and *Marsh et al.* [2007] show very similar winter/summer distributions from their climate model simulations. Note, however, that the meridional gradients of H_2O in Fig. 10 for the winter hemisphere are larger in northern hemisphere (NH) than in the southern hemisphere (SH), related possibly to the asymmetry in the AO amplitudes across the two hemispheres (Fig. 6). Meridional wave mixing processes will be more effective for the net transport of H_2O in the NH. Further, the responses to MEI are smaller in Fig. 9 for the lower mesosphere, where the meridional H_2O gradients are small in Fig. 10.

MLR analyses of CH_4, a companion tracer of H_2O, yield responses that are also significant but positive at 0.7 hPa across all latitudes (Table 2—top rows). Inclusion of the ENSO term improves the MLR model fit to the time series of HALOE CH_4 data shown earlier by *Remsberg* [2015]. Such anti-correlated responses between CH_4 and H_2O are because the mixing ratio gradients for CH_4 are opposite those of H_2O from Equator to Pole near the stratopause. In summary, the response distribution of H_2O in Fig. 9 represents further evidence for the combined roles of planetary and gravity wave forcings and the effects of their dissipation for transport and mixing in the mesosphere.

5. Responses of H_2O to solar forcings

One ought to be able to gain quantitative estimates of the responses of H_2O in the upper mesosphere to variations of the Ly-α flux from a single, 11-yr solar cycle because the associated trends for H_2O in that region are small in comparison and will have almost no effect on the analyzed H_2O coefficients of the Lya terms. Figure 11 shows the distribution of the annual average response of H_2O to the maximum minus minimum forcings of the Ly-α flux (as a percentage of the annually averaged, or the constant terms of Figure 1). That response is uniformly negative in the upper mesosphere because of photolysis from the enhanced Ly-α flux at solar maximum. Smallest responses occur at the low latitudes, where the Sun is more nearly overhead in the annual average. We do not show H_2O responses to solar max minus min for solstice because the terms of the MLR analyses are not from time series of just that season.

The distribution in Figure 11 indicates that the responses decline to zero at about 0.1 hPa and then change to weakly positive in the low to middle mesosphere in the SH tropics and subtropics. Solar responses are negative throughout the northern hemisphere, perhaps a result of dynamical effects that are a somewhat larger in that region and may be overwhelming them. Even though the positive and negative responses are of small amplitude and not highly significant, their patterns are the result of separate MLR analyses at each latitude and pressure-altitude location. Continuity of the responses to Ly-α across that region is an indicator of the fidelity of the distribution in Fig. 11.

Positive responses at solar flux maximum occur from the greater production of O (^{1}D) and ozone following the UV-photolysis of O_2 in the Schumann-Runge bands and in the Herzberg continuum or the wavelength range of $190 < \lambda < 235$ nm [*Nicolet*, 1981]. O (^{1}D) reacts with H_2O and H_2 and with CH_4 in the upper stratosphere, generating odd hydrogen (HO_x = OH + HO_2 + H). Both CH_4 and H_2 then react with OH to give H_2O [*Brasseur and Solomon*, 2005]. The combination of CH_4 and OH gives formaldehyde (CH_2O) and H_2O, and CH_2O reacts to produce H_2O, as well, via a sequence of reactions [e.g., *Remsberg et al*., 1984]. As an example, *Natarajan et al.* [1981] calculated a decrease of 18% for CH_4 at 55 km from a 1-D model having a top level of 60 km. They also obtained increases at that level of order 20% for O, O (^{1}D), and HO_x and an increase of 9% for H_2O at solar maximum.

Separate MLR analyses for the solar cycle response in HALOE CH_4 at the 1.0-hPa level (or near the stratopause) yield ~5 to 12% less CH_4 for solar maximum minus minimum from 52.5°S to 7.5°N (with CI ~70%), but 4 to 7% more CH_4 for 22.5°N to 37.5°N (see Table 2—bottom rows). Thus, there is an observed anti-correlation of the responses in HALOE H_2O and CH_4 at solar flux maximum in the lowermost mesosphere of the southern hemisphere. A part of the excess of H_2O

produced at the stratopause undergoes net ascent to the middle mesosphere [*Brasseur and Solomon*, 2005]. Note that the upward bulge of the zero response contour in Figure 11 extends to 0.1 hPa or near to the location of the H_2O maximum in Figure 1.

6. Linear trends in H_2O

Figure 12 is the distribution of the associated linear trends for H_2O (in %/decade), as analyzed with the MLR models. While there are significant, positive trends of > 1.5 %/decade through most of the mesosphere at the middle latitudes, the trends at the low latitudes are small (within ±1.5 %/decade from about 25°S to 25°N latitudes) and not significantly different from zero. They are also small (less than about 1.5 %/decade) in the lowermost mesosphere even at the middle latitudes. The H_2O trends of Fig. 12 are smaller than the secular trends from the model study of *Garcia et al*. [2007] and somewhat smaller than the analyzed trends of the HALOE data in *Randel et al*. [2004], both for the time span of 1992-2002. On the other hand, *Nedoluha et al.* [2017] reported on H_2O trends at 0.46 hPa for 1996 through 2005 from two ground-based microwave measurement sites (Mauna Loa, Hawaii at 19.5°N, 204°E and Lauder, New Zealand at 45°S, 170°E). Their trends are between ±1 %/decade and are consistent with observed trends of H_2O entering the stratosphere. Prior to 1996, their H_2O trends are increasing in the lower mesosphere. Overall, the linear trends of Fig. 12 agree with their reported findings.

As indicated earlier, a significant fraction of the H_2O reaching the lowermost mesosphere comes from the oxidation of CH_4. CH_4 mixing ratios at 0.7 hPa are small, varying between 0.34 and 0.19 ppmv from low to higher latitudes. Their corresponding MLR analyses yield trends of the order of 6 %/decade at 0.7 hPa, although they are not highly significant. Observed trends for ground-level CH_4 were a bit larger than that for the 1980s, but they became variable and generally smaller in the 1990s and early 2000s [*Dlugokencky et al*., 2009].

The analyzed trends of HALOE H_2O in Fig. 12 are significant and greater than 4.5%/decade at middle to high latitudes of the upper mesosphere. They are also larger than the observed trends for H_2O and CH_4 in the stratosphere. One explanation for such large trends is that the Ly-α flux was sustained and of the order of 6.0 flux units throughout 1991 and early 1992, whereas it only reached 5.9 units and for just a few months in late 2001 to early 2002. Thus, it is likely that H_2O was subject to enhanced photolysis prior to the start time of mid-1992 for the present analysis of the HALOE time series, and the rather large, positive trends at the high latitudes represent a recovery from lower H_2O values of 1991 in that region. A single linear trend is inadequate for characterizing that anomaly for the start of the time series.

7. Sensitivity to bias errors

Separate analyses using the simultaneous temporal and spatial analyses (STS) method of *Damadeo et al.* [2017] indicate whether there are any biases affecting the results of the HALOE data series. The STS analyses are for data time series that include seasonal, QBO, Lya, ENSO, and linear trend terms. In this model, the QBO variations are according to two orthogonal terms scaled from variations of the tropical QBO winds, and the solar forcings are according to the 10.7 cm flux proxy. The solar and ENSO responses and the trends from the STS approach (not shown) are very similar to those reported in Sections 5 and 6, even the rather large trends of Fig. 12 at the higher latitudes. Both diurnal (SR/SS) and latitudinal sampling biases are small and not significant throughout most of the mesosphere.

An exception is that the STS method reveals systematic SS/SR differences for H_2O in the uppermost mesosphere, although they are not of the same sign across all latitudes. For example, separate analyses of the SS and SR time series data at 37.5°N (Fig. 2) yield differences for their constant terms of -13% (SS minus SR), and where maximum seasonal H_2O values tend to be measured during a SR occultation event. Conversely, the SS minus SR H_2O differences change sign to +4% in the tropics. Figure 13 summarizes the H_2O differences. They vary symmetrically with latitude about the Equator and are anti-correlated with those of temperature. Such variations occur in the data, although they are not significant because of the very large random error for single H_2O profiles in the uppermost mesosphere [*Harries et al.,* 1996, their Table 1].

The foregoing SS/SR response variation with latitude seems unphysical for atmospheric H_2O, and it is largest where the vertical gradient of H_2O is strongly negative in Fig. 1 (at 0.01 and 0.015 hPa). The anti-correlation of H_2O and temperature in Fig. 13 suggest that these HALOE H_2O responses vary with the phase of the atmospheric temperature tides, which also vary with latitude. In addition, tropical SS minus SR H_2O becomes negative (-4%) at 0.15 hPa, or just where SS minus SR temperatures are +6 K. Such a change with altitude is in accord with the vertical half-wavelength of the diurnal temperature tide. Since vertical resolution for HALOE-retrieved H_2O is 2.3 km versus ~4 km for its temperature, this mismatch affects the pressure-registration of the H_2O transmittance profile and carries over to the retrieval of the H_2O mixing ratio profile. Simulation studies show that there is also some dampening of vertical temperature structures due to tides and inversion layers in the HALOE data. The HALOE retrieval algorithm for T(p) iterates only three times and does not resolve those structures fully, leading to vertical variations for retrieved H_2O that are of the opposite sign [*Remsberg* et al., 2002, their Section 5]. While such tropical SS/SR differences are characteristic of the HALOE-retrieved H_2O in those circumstances, an MLR analysis of time series of HALOE SS plus SR H_2O data points still yields representative results for all the terms of the MLR model in Eq. (1). This is because the associated AR1 coefficient is slightly negative in that instance, and the two-step, MLR analysis method corrects for that occurrence.

Figure 14 shows a time series for the lower mesosphere (0.7 hPa) at 22.5°S, where the trend coefficient for H_2O is small (-0.9 %/decade) and not significant. The AR1 coefficient is positive (0.24) from the residuals of the initial MLR fit, indicating some memory at lag-1. One can also see that the HALOE H_2O data of 1991-92 in Fig. 14 have values that are lower than the linear trend line by about 0.4 ppmv. *Fueglistaler* [2012] also found lower values in the tropics at 10 hPa for total water or the sum of H_2O and $2*CH_4$ in 1991-92. He traced those values to the lower H_2O that had entered the stratosphere some months before the eruption of Pinatubo. Thus, the low values at 0.7 hPa are likely the result of a net ascent of relatively dry air from 10 hPa with a lag time of a year or so. Somewhat smaller H_2O values at the beginning of the HALOE data record of Fig. 14 represent a bias or end-point anomaly for the trend term as well as for the determination of the coefficient of the Lya term. Use of the delayed start date of July 1992 reduces the effect of that bias for the analyses herein.

8. Comparisons with previous analyses of H_2O

Figure 15 shows the seasonal, ENSO, and Lya response profiles from HALOE, as averaged across the four low latitude bins spanning 30°S to 30°N. Horizontal bars at selected pressure levels represent their 1-σ uncertainties. These average HALOE response profiles compare reasonably with the ones of *Nath et al.* [2017, their Figures 5 and 7] for the middle and upper mesosphere based on AURA MLS data of 2004 to 2015. There are differences in several regions, however. AO amplitudes from HALOE are about 0.1 ppmv and not significant from 0.2 to 0.7 hPa, while those from MLS grow from 0.1 to 0.3 ppmv from the middle mesosphere to near the stratopause. Notably, MLS H_2O has amplitudes of about 0.3 ppmv for both the SAO and AO terms, while those from HALOE remain of order 0.1 ppmv. The AR1 coefficient is ~0.3 near the stratopause, which dampens the HALOE AO and SAO amplitudes by about 30%. The data time series from MLS may be more representative of zonal average H_2O than are those of HALOE, especially in the tropics where Kelvin (zonal wave-1) waves occur. Therefore, we checked to see whether increasing the minimum number to profiles in a latitude bin from 5 to 8 was affecting our HALOE results, but we found little difference. It may be that the differing vertical resolutions and retrieval algorithm approaches for H_2O of HALOE and MLS are contributing to their amplitude differences [e.g., *Harries et al.*, 1996; *Lambert et al.*, 2007]; further estimates of them are not part of this study. There is also a notable difference in the H_2O responses to MEI for the uppermost mesosphere. *Nath et al.* [2017] report a significant positive response of 0.1 ppmv/MEI at 0.01 hPa. Instead, Fig. 15 shows a near zero value for the coefficient of that term, although it is not significant because the HALOE-retrieved H_2O has large random errors at that pressure-level.

Initially, *Remsberg* [2010] used an 11-yr (or SC-like) term in his MLR modeling and reported finding that H_2O had maximum values at solar minimum in the uppermost mesosphere or at about 5.5 years from January 1991. He also found that H_2O maximum lagged solar minimum by up to 2 years in the tropical middle mesosphere (0.15 hPa) but noted that the phase of the 11-yr term was sensitive to his associated, collinear trend term. To check about that, we perform analysis at 7.5°S and 0.15 hPa first using the 11-yr term in the model and then using the Lya term, both analyses having a start time of July 1992. Although the respective linear trends are about equal (-1.4 %/decade), the H_2O response to max minus min for the 11-yr term is -4.4% while the equivalent response to Ly-α is +1.1%. The H_2O model response to Ly-α should be more accurate because it is insensitive to the trend term and because the Ly-α flux series is a better representation of the solar flux variations than the 11-yr sinusoid. On the other hand, the analyzed H_2O response to Ly-α becomes slightly negative (-1.3%) instead of slightly positive (+1.1%) upon using an analysis start time of day 300 or late 1991 instead of day 547 (July 1992). This difference represents the effects of the sustained and slightly larger flux values of late 1991-mid 1992, as compared with the fluxes in early 2002.

9. Conclusions

Multiple linear regression (MLR) analysis is re-applied to time series of HALOE H_2O from July 1992 through November 2005 for the latitudes of 60°S to 60°N and for the mesosphere (0.01 to 1.0 hPa). Two separate MLR approaches are considered, and both of them analyze all the relevant terms together rather than using de-seasonalized residuals. The first MLR model considers regressing the data separately at each latitude and pressure bin, where the solar cycle forcing is from the concurrent Ly-α flux time series. Largest seasonal and solar cycle variations in H_2O occur in the upper mesosphere. As expected, there is a strong anti-correlation between H_2O and the solar cycle flux forcing. The second approach is a two-dimensional regression applied to the HALOE SR and SS data as they occur sequentially, and it accounts for diurnal effects, data gaps, and any long-term changes in the sampling with latitude of the HALOE measurements. The analyzed responses of HALOE H_2O to the Ly-α flux have very similar patterns and magnitudes from both approaches. We also find good agreement with the analogous responses at the low latitudes and the middle and upper mesosphere from the MLS H_2O data, as reported by *Nath et al.* [2017].

H_2O is an effective tracer of the seasonal and interannual variations in the mesosphere via its responses to the net circulation. Annual cycle variations of H_2O and temperature have similar asymmetries in the upper mesosphere, suggesting hemispheric differences in their dynamical forcings. There are also significant negative H_2O responses in the northern hemisphere to the time series of the ENSO index, and they are anti-correlated with those for temperature. Those findings indicate the anomalous effects of wave dissipation for the net circulation, particularly in the upper mesosphere. The responses of H_2O to solar Ly-α forcings are large and anti-phased throughout the upper mesosphere. However, that same term also shows very weak, positive H_2O responses in the tropical middle and lower mesosphere at solar flux maximum. Positive responses suggest effects of the enhanced photolysis of O_2 at solar maximum near the stratopause, leading to the oxidation of CH_4 and generation of H_2O, and followed by a net vertical transport to the tropical middle mesosphere. The associated H_2O trends are near zero from HALOE for 1992 to 2005 and agree reasonably with separate, published observational trends for H_2O and for its stratospheric source gas CH_4. Findings from these re-analyses ought to be useful diagnostics for the verification of chemistry-climate models of the mesosphere.

Acknowledgements. HALOE data are from (*http://haloe.gats-inc.com/home/index.php/*), daily Ly-α fluxes are from (*http://lasp.colorado.edu/lisird/lya/*), and ENSO MEI values are from (*https://www.esrl.noaa.gov/psd/enso/mei/*). R. Earl Thompson conducted the simulations studies with bias errors in HALOE temperature profiles and the propagation of those effects to the retrievals of H_2O. ER and MN performed this work as Distinguished Research Associates (DRA) at NASA Langley.

References

Andrews, D. G., J. R. Holton, and C. B. Leovy (1987), *Middle Atmosphere Dynamics*, 489 pp., Academic Press, Inc., Orlando, Florida.

Baldwin, M. P., L. J. Gray, T. J. Dunkerton, K. Hamilton, P. H. Haynes, W. J. Randel, J. R. Holton, M. J. Alexander, I. Hirota, T. Horinouchi, D. B. A. Jones, J. S. Kinnersley, C. Marquardt, K. Sato, M. Takahashi (2001), The quasi-biennial oscillation, Rev. Geophys., 39, 179-229, doi: 10.1029/1999RG000073.

Brasseur, G., and S. Solomon (2005), *Aeronomy of the Middle Atmosphere: Chemistry and Physics of the Stratosphere and Mesosphere*. 3rd ed., 644 pp., Springer, Dordrecht, Netherlands.

Chandra, S., C. H. Jackman, E. L. Fleming, and J. M. Russell III (1997), The seasonal and long term changes in mesospheric water vapor, *Geophys. Res., Lett., 24*, 639-642, doi:10.1029/97GL00546.

Cochrane, D. and G. Orcutt (1949), Application of least squares regression to relationships containing auto-correlated error terms, *J. Am. Stat. Assoc.*, *44*, 32–61, doi:10.1080/01621459.1949.10483290.

Damadeo, R., J. Zawodny, E. Remsberg, and K. Walker (2017), The Impact of Non-uniform Sampling on Stratospheric Ozone Trends Derived from Occultation Instruments, *Atmos. Chem. Phys. Discuss.*, doi.org/10.5194/acp-2017-575.

Dlugokencky, E. J., L. Bruhwiler, J. W. C. White, L. K. Emmons, P. C. Novelli, S. A. Montzka, K. A. Masarie, P. M. Lang, A. M. Crotwell, J. B. Miller, and L. V. Gatti (2009), Observational constraints on recent increases in the atmospheric CH_4 burden, *Geophys. Res. Lett., 36*, L18803, doi:10.1029/2009GL039780.

Fueglistaler, S. (2012), Stepwise changes in stratospheric water vapor?, *J. Geophys. Res., 117*, D13302, doi:10.1029/2012JD017582.

Garcia, R. R., S. Solomon, R. G. Roble, and D. W. Rusch (1984), A numerical response of the middle atmosphere to the 11-year solar cycle, *Planet. Space Sci., 32,* 411-423, doi:10.1016/0032-0633(84)90121-1.

Garcia, R. R., D. R. Marsh, D. E. Kinnison, B. A. Boville, and F. Sassi (2007), Simulation of secular trends in the middle atmosphere, 1950-2003, *J. Geophys. Res.*, *112*, D09301, doi:10.1029/JD007485.

Gordley, L., E. Thompson, M. McHugh, E. Remsberg, J. Russell III, and B. Magill (2009), Accuracy of atmospheric trends inferred from the Halogen Occultation Experiment data, *J. Appl. Remote Sens., 3,* doi:10.1117/1.3131722.

Grooss, J.-U., and J. M. Russell III (2005), Technical note: A stratospheric climatology for O_3, H_2O, CH_4, NO_x, HCl and HF derived from HALOE measurements, *Atmos. Chem. Phys., 5*, 2797-2807, 1680-7324/acp/2005-5-2797.

Harries, J. E., J. M. Russell III, A. F. Tuck, L. L. Gordley, P. Purcell, K. Stone, R. M. Bevilacqua, M. Gunson, G. Nedoluha, and W. A. Traub (1996), Validation of measurements of water vapor from the Halogen Occultation Experiment (HALOE), *J. Geophys. Res., 101*, D6, 10,205-10,216, doi: 10.1029/95JD02933.

Hervig, M. E., and D. Siskind (2006), Decadal and inter-hemispheric variability in polar mesospheric clouds, water vapor, and temperature, *J. Atmos. Solar-Terr. Phys.*, *68*, 30-41, doi:10.1016/jastp.2005.08.010.

Kley, D., J. M. Russell III, and C. Phillips (Eds.) (2000), *SPARC assessment of upper tropospheric and stratospheric water vapour,* World Climate Research Programme (WCRP) Rep. 113, World Clim. Res. Programme, 312 pp., Geneva, Switzerland.

Lambert, A., W. G. Read, N. J. Livesey, M. L. Santee, G. L. Manney, L. Froidevaux, D. L. Wu, M. J. Schwartz, H. C. Pumphrey, C. Jimenez, G. E. Nedoluha, R. E. Cofield, D. T. Cuddy, W. H. Daffer, B. J. Drouin, R. A. Fuller, R. F. Jarnot, B. W. Knosp, H. M. Pickett, V. S. Perun, W. V. Snyder, P. C. Stek, R. P. Thurstans, P. A. Wagner, J. W. Waters, K. W. Jucks, G. C. Toon, R. A. Stachnik, P. F. Bernath, C. D. Boone, K. A. Walker, J. Urban, D. Murtagh, J. W. Elkins, and E. Atlas (2007), Validation of the Aura Microwave Limb Sounder middle atmosphere water vapor and nitrous oxide measurements, *J. Geophys. Res.*, *112,* D24S36, doi:10.1029/2007JD008724.

Lee, H., and A. K. Smith (2003), Simulation of the combined effects of solar cycle, quasi-biennial oscillation, and volcanic forcing on stratospheric ozone changes in recent decades, *J. Geophys. Res.*, *108*, D2, 4049, doi:10.1029/2001JD001503.

Li, T., T. Leblanc, and I. S. McDermid (2008), Interannual variations of middle atmospheric temperature as measured by the JPL lidar at Mauna Loa Observatory, Hawaii (19.5°N, 155.6°W), *J. Geophys. Res.*, *113*, D14109, doi:10.1029/2007JD009764.

Li, T., N. Calvo, J. Yue, X. Dou, J. M. Russell III, M. G. Mlynczak, C.-Y. She, and X. Xue (2013), Influence of El Niño-Southern Oscillation in the mesosphere, *Geophys. Res. Lett.*, *40*, 3292-3296, doi:10.1002/grl.50598.

Li, T., N. Calvo, J. Yue, J. M. Russell III, A. K. Smith, M. G. Mlynczak, A. Chandran, X. Dou, and A. Z. Liu (2016), Southern hemisphere summer mesopause responses to El Niño-Southern Oscillation, *J. Climate*, *29*, 6319-6328, doi:10.1175/JCLI-D-15-0816.1.

Lossow, S., J. Urban, J. Gumbel, P. Eriksson, and D. Murtagh (2008), Observations of the mesospheric semi-annual oscillation (MSAO) in water vapour by Odin/SMR, *Atmos. Chem. Phys.*, *8*, 6527-6540, https://doi.org/10.5194/acp-8-6527-2008.

Marsh, D. R., R. R. Garcia, D. E. Kinnison, B. A. Boville, F. Sassi, S. C. Solomon, and K. Matthes (2007), Modeling the whole atmosphere response to solar cycle changes in radiative and geomagnetic forcing, *J. Geophys. Res.*, *112*, D23306, doi:10.1029/2006JD008306.

Natarajan, M., L. B. Callis, and J. E. Nealy (1981), Solar uv variability: effects on stratospheric ozone, trace constituents and thermal structure, *PAGEOPH*, *119*, 750-779.

Nath, O., S. Sridharan, and C. V. Naidu (2017), Seasonal, interannual and long-term variabilities and tendencies of water vapour in the upper stratosphere and mesospheric region over tropics (30°N-30°S), *J. Atmos. Solar Terr. Phys.*, http://dx.doi.org/10.1016/j.jastp.2017.07.009.

Nedoluha, G. E., M. Kiefer, S. Lossow, R. M. Gomez, N. Kämpfer, M. Lainer, P. Forkman, O. M. Christensen, J. J. Oh, P. Hartogh, J. Anderson, K. Bramstedt, B. M. Dinelli, M. Garcia-Comas, M. Hervig, D. Murtagh, P. Raspollini, W. G. Read, K. Rosenlof, G. P. Stiller, and K. A.

Walker (2017), The SPARC water vapor assessment II: intercomparison of satellite and ground-based microwave measurements, *Atmos. Chem. Phys. Discuss.*, https://doi.org/10.5194/acp-2017-578.

Nedoluha, G. E., R. M. Gomez, B. C. Hicks, J. E. Wrotny, C. Boone, and L. Lambert (2009), Water vapor measurements in the mesosphere from Mauna Loa over solar cycle 23, *J. Geophys. Res., 114*, D23303, doi:10.1029/2009JD012504.

Nicolet, M. (1981), The photodissociation of water vapor in the mesosphere, *J. Geophys. Res.*, *86*, 5203-5208, doi:10.1029/JC086iC06p05203.

Palo, S. E., J. M. Forbes, X. Zhang, J. M. Russell III, C. J. Mertens, M. G. Mlynczak, G. B. Burns, P. J. Espy, and T. D. Kawahara (2005), Planetary wave coupling from the stratosphere to the thermosphere during the 2002 southern hemisphere pre-stratwarm period, *Geophys. Res. Lett., 32*, L23809, doi:10.1029/2005GL024298.

Randel, W. J., F. Wu, J. M. Russell III, J. M. Zawodny, and J. Nash (2000), Interannual changes in stratospheric constituents and global circulation derived from satellite data, in *Atmospheric Science Across the Stratopause*, AGU Geophysical Monograph 123, 271-285.

Randel, W. J., F. Wu, S. J. Oltmans, K. Rosenlof, and G. E. Nedoluha (2004), Interannual changes in stratospheric water vapor and correlations with tropical tropopause temperatures, J. Atmos. Sci., 61, 2133-2148.

Remsberg, E. E. (2015), Methane as a diagnostic tracer of changes in the Brewer-Dobson circulation of the stratosphere, *Atmos. Chem. Phys.*, *15*, 3739-3754, doi:10.5194/acp-15-3739-2015.

Remsberg, E. (2010), Observed seasonal to decadal scale responses in mesospheric water vapor, *J. Geophys. Res.*, *115*, D06306, doi:10.1029/2009JD012904.

Remsberg, E. (2007), A reanalysis for the seasonal and longer-period cycles and the trends in middle-atmosphere temperature from the halogen occultation experiment, *J. Geophys. Res.*, *112*, D09118, doi:10.1029/2006JD007489.

Remsberg, E., L. Deaver, J. Wells, G. Lingenfelser, P. Bhatt, L. Gordley, R. Thompson, M. McHugh, J. M. Russell III, P. Keckhut, and F. Schmidlin (2002), An assessment of the quality of Halogen Occultation Experiment temperature profiles in the mesosphere based on comparisons with Rayleigh backscatter lidar and inflatable falling sphere measurements, *J. Geophys. Res.*, *107*, D20, 4447, doi:10.1029/2001JD001521.

Remsberg, E. E., P. P. Bhatt, and J. M. Russell III (1996), Estimates of the water vapor budget of the stratosphere from UARS HALOE data, *J. Geophys. Res.*, *101*, 6749-6766, 95JD03858.

Remsberg, E. E., J. M. Russell III, L. L. Gordley, J. C. Gille, and P. L. Bailey (1984), Implications of the stratospheric water vapor distribution as determined from the Nimbus 7 LIMS experiment, *J. Atmos. Sci.*, *41*, 2934-2945, doi: http://dx.doi.org/10.1175/1520-0469(1984)041<2934:IOTSWV>2.0.CO;2.

Russell III, J. M., L. L. Gordley, J. H. Park, S. R. Drayson, W. D. Hesketh, R. J. Cicerone, A. F. Tuck, J. E. Frederick, J. E. Harries, P. J. Crutzen (1993), The halogen occultation experiment, *J. Geophys. Res., 98,* 10777-10797, doi: 10.1029/93JD00799.

Schmidt, H., G. P. Brasseur, M. Charron, E. Manzini, M. A. Giorgetta, T. Diehl, V. I. Fomichev, D. Kinnison, D. Marsh, and S. Walters (2006), The HAMMONIA chemistry climate model: sensitivity of the mesopause region to the 11-year solar cycle and CO_2 doubling, *J. Climate, 19*, 3903-3931, doi:10.1175/JCLI3829.1.

She, C. Y., S. W. Thiel, and D. A. Kreuger (1998), Observed episodic warming at 86 and 100 km between 1990 and 1997: effects of Mount Pinatubo eruption, *Geophys. Res. Lett., 25*, 497-500, doi: 10.1029/98GL00178.

Tiao, G. C., G. C. Reinsel, D. Xu, J. H. Pedrick, X. Zhu, A. J. Miller, J. J. DeLuisi, C. L. Mateer, and D. J. Wuebbles (1990), Effects of autocorrelation and temporal sampling schemes on estimates of trend and spatial correlation, *J. Geophys. Res., 95*, 20,507-20,517, doi:10.1029/JD095iD12p20507.

Table 1. Coefficients and Confidence Intervals of MLR H_2O Model Terms for 37°N, 0.015 hPa

Term	*Coefficient (ppmv)*	*Std. Dev., σ (ppmv)*	*CI (%)*
Constant	3.65	---	---
Annual (AO)	-1.34	0.12	99
Semi-annual (SAO)	0.40	0.07	99
QBO-like (QBO)	-0.02	0.07	22
Solar flux (Lya)#	-0.56	0.05	99
MEI (ENSO)#	-0.26	0.06	99
*Linear Trend (Lin)**	0.18	0.03	96

*Coefficient and σ of *Lin* term are in units of ppmv-decade^{-1}. #Solar flux and MEI coefficients have units of ppmv but are with respect to normalized (-1 to +1) proxy time series.

Table 2. Methane response (CH_4 in % MEI^{-1}) at 0.7 hPa to forcings according to the ENSO index and CH_4 response (in %) at 1.0 hPa to solar max minus solar min.

Latitude	52.5S	37.5	22.5	7.5S	7.5N	22.5	37.5	52.5N
CH_4(0.7hPa)								
ppmv MEI^{-1}	0.013	0.017	0.010	0.009	0.013	0.017	0.015	0.016
% MEI^{-1}	6.5	6.5	3.4	3.2	4.3	5.0	5.2	8.4
CI (%)	99	99	99	99	99	99	99	99
CH_4(1.0hPa)								
Max – Min (ppmv)	-0.016	-0.015	-0.036	-0.042	-0.028	0.032	0.015	-0.022
Lya (%)	-7.4	-5.2	-10.3	-12.0	-7.6	7.4	4.4	-10.0
CI (%)	68	59	81	69	63	67	28	78

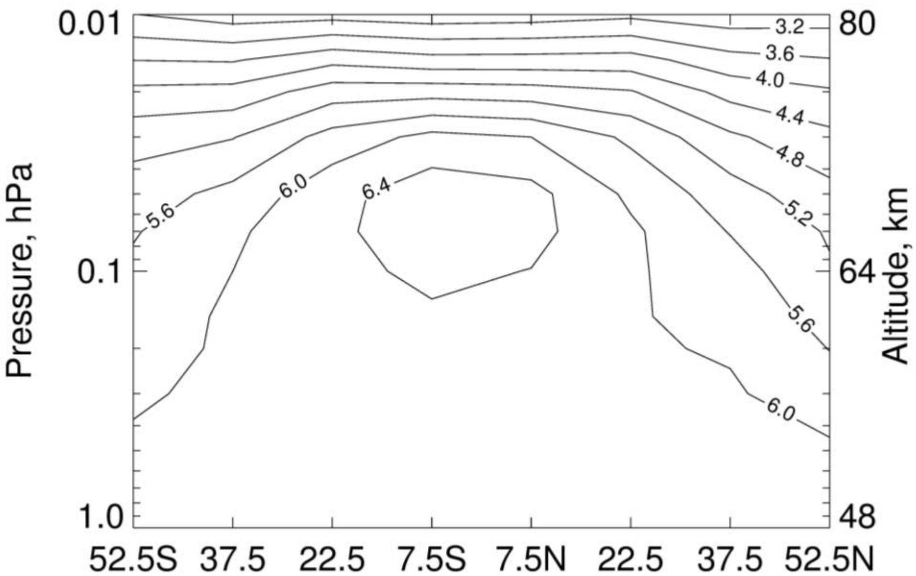

Figure 1—Pressure versus latitude contour plot of the average estimate of H_2O mixing ratios (in ppmv) from time series of HALOE data for July 1992 to November 2005. Contour interval is 0.4 ppmv; altitude coordinate is approximate.

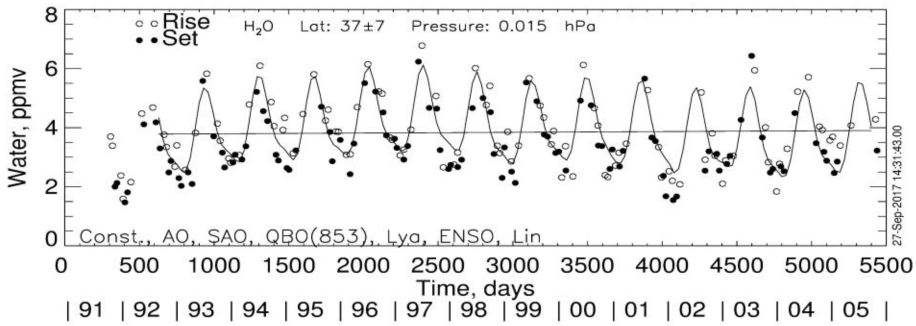

Figure 2—Time series of bin-averaged HALOE sunset (SS, solid circles) and sunrise (SR, open circles) H_2O values at 37.5°N and 0.015 hPa (near 75 km). The oscillating curve is the multiple linear regression model fit to those values.

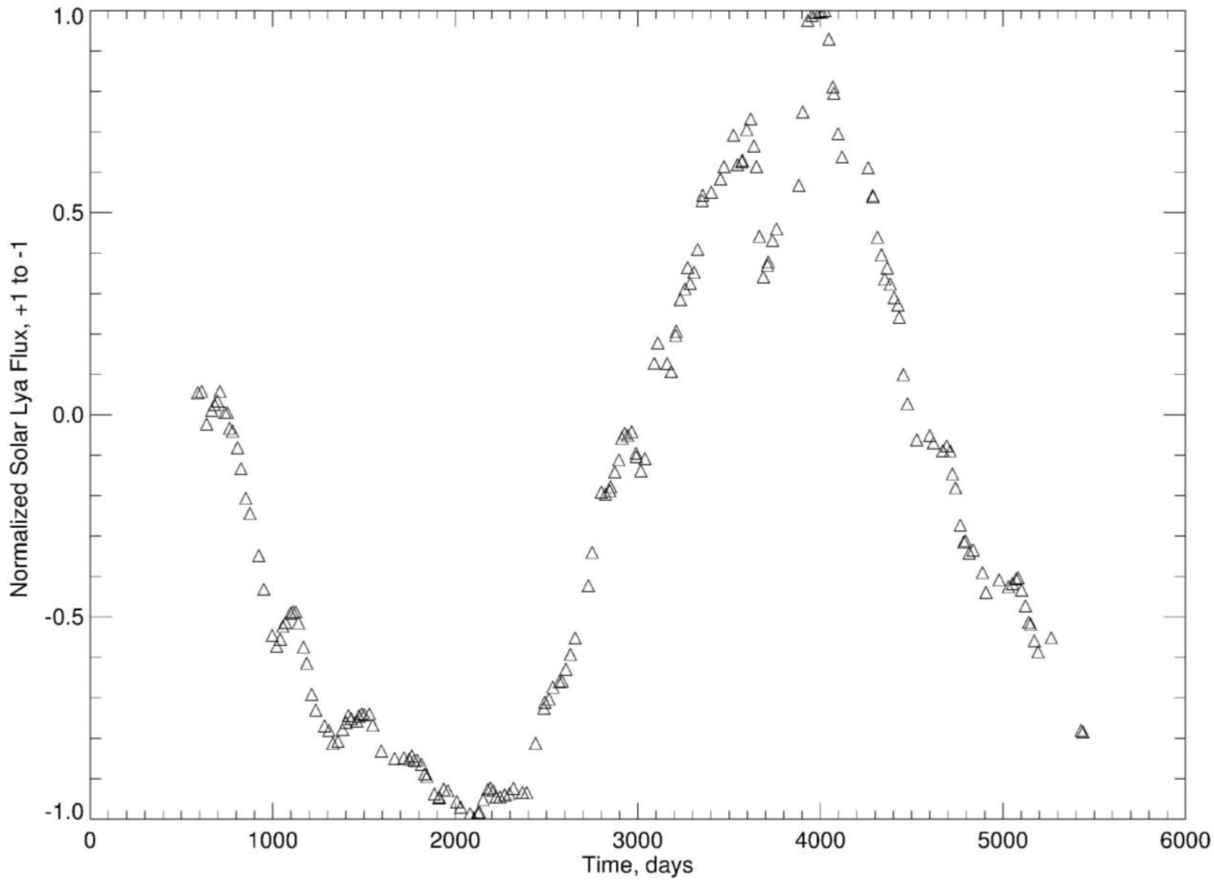

Figure 3—Discrete time series of the normalized, Ly-α flux that matches the data points of Figure 2 for July 1992 onward.

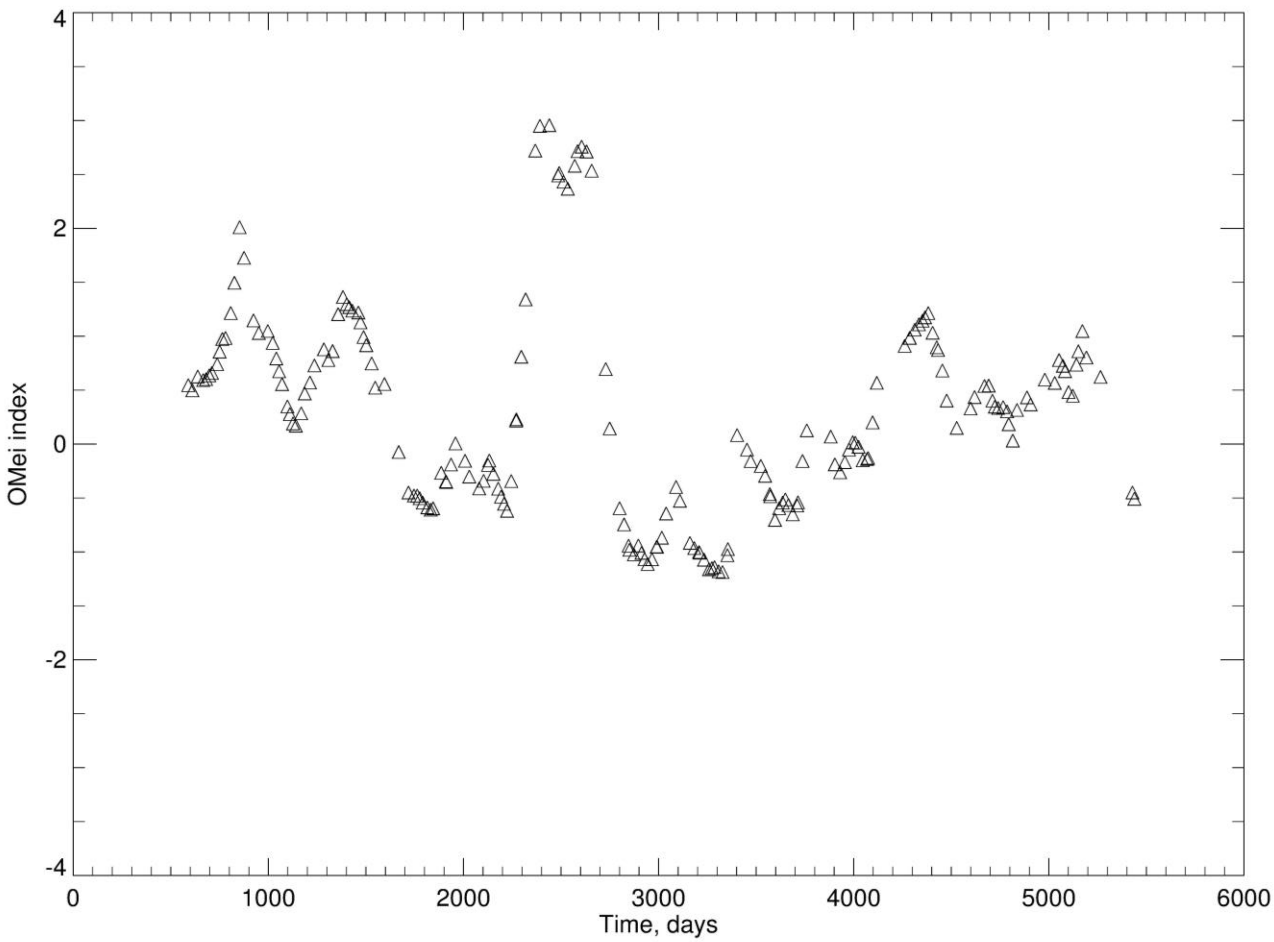

Figure 4—Discrete time series of the MEI index that matches the data of Figure 2.

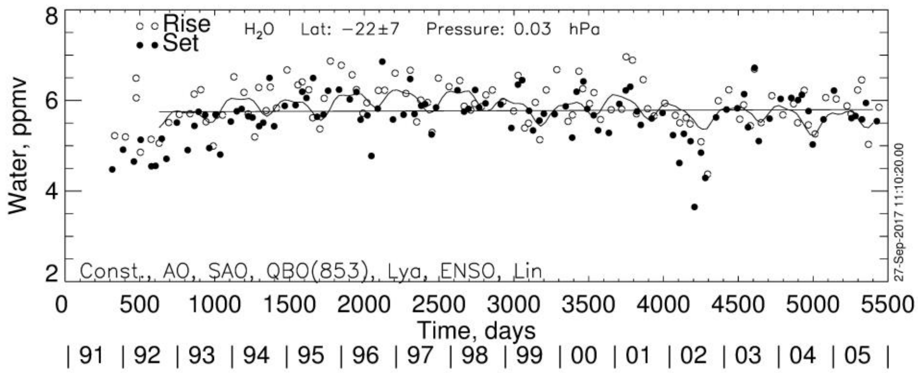

Figure 5—As in Figure 2, but for 22.5°S and 0.03 hPa.

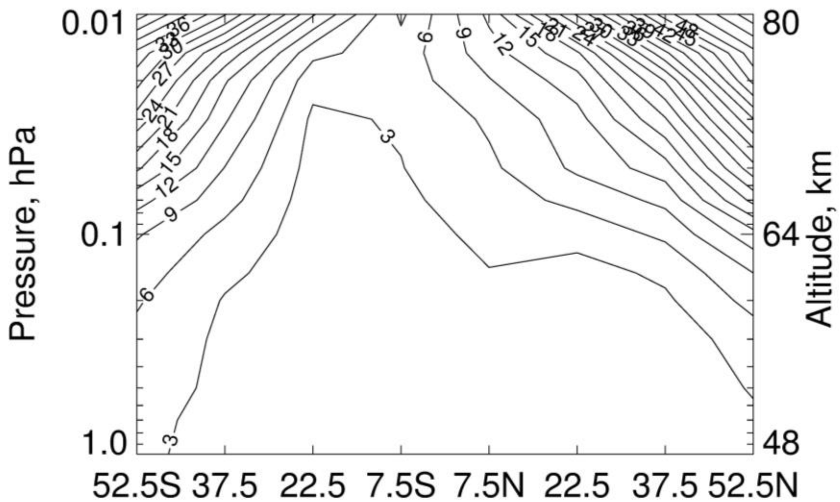

Figure 6—Amplitudes of the annual oscillation terms, as a percentage of the H_2O mixing ratios in Figure 1. Contour interval is 3%.

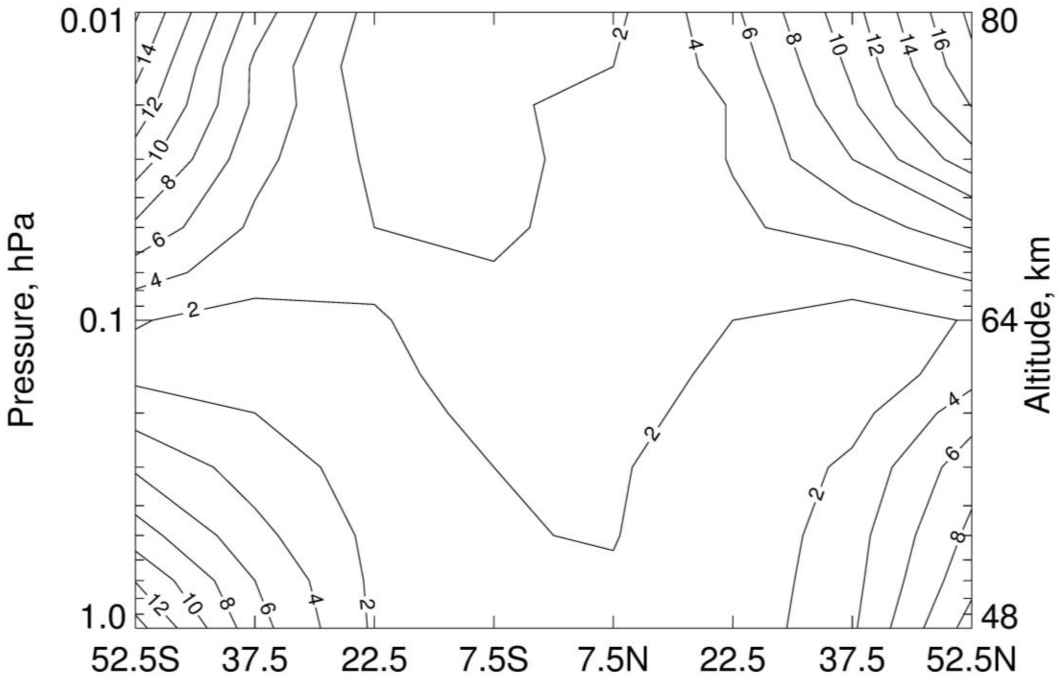

Figure 7—Distribution of the amplitudes of the annual oscillation (AO) for temperature from HALOE. Contour interval is 2 K.

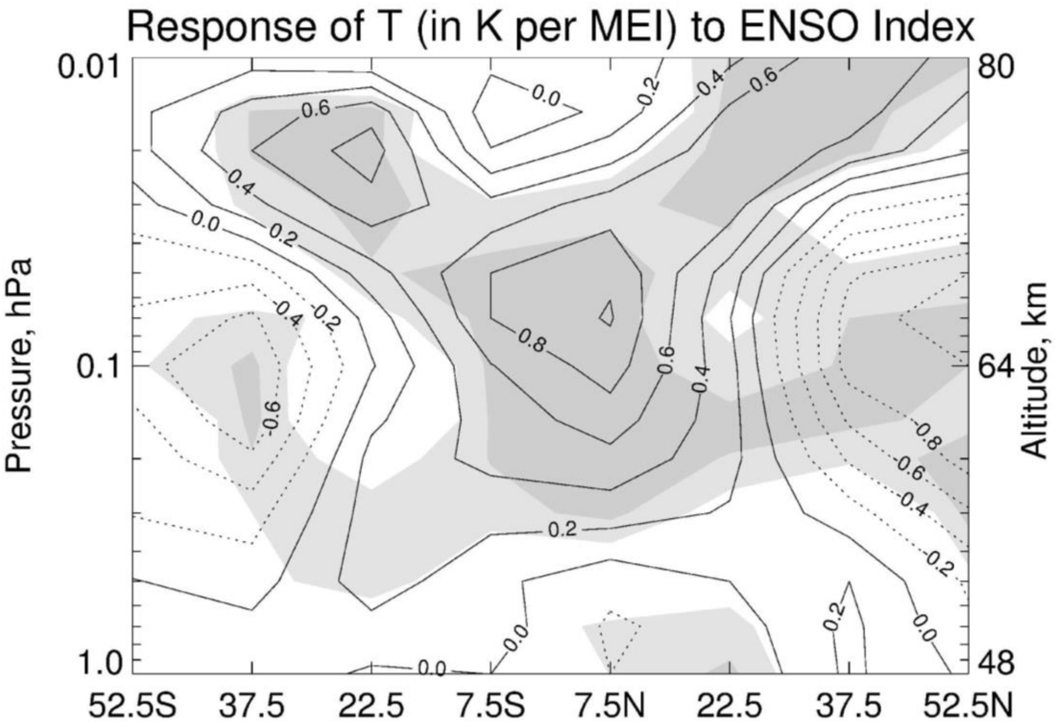

Figure 8—Distribution of the responses of temperature to the forcings from ENSO. Solid contours represent zero and positive responses, and contour interval is 0.2 K MEI^{-1}. Darker shading denotes regions where there is > 90% confidence interval (CI) for the terms being present in the data; lighter shading denotes where the terms have a 70% < CI < 90%.

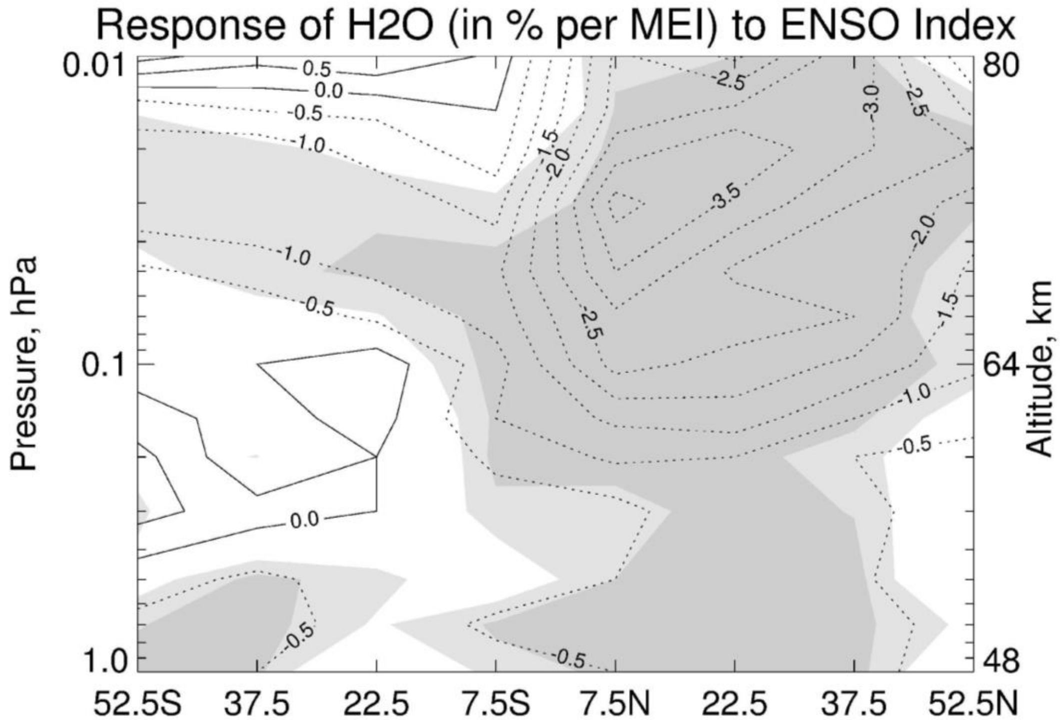

Figure 9—Distribution of the responses of H_2O to the forcings from ENSO (in terms of % of the H_2O mixing ratios of Fig. 1). Dashed contours are negative and contour interval is 0.5%. CI values are as in Fig. 8.

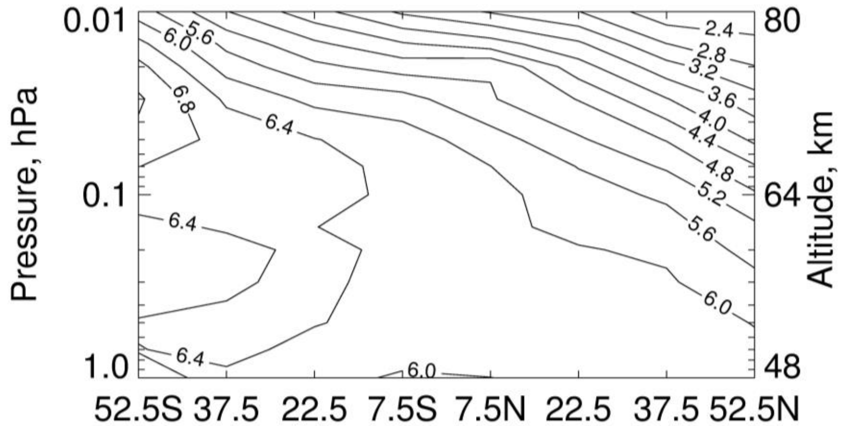

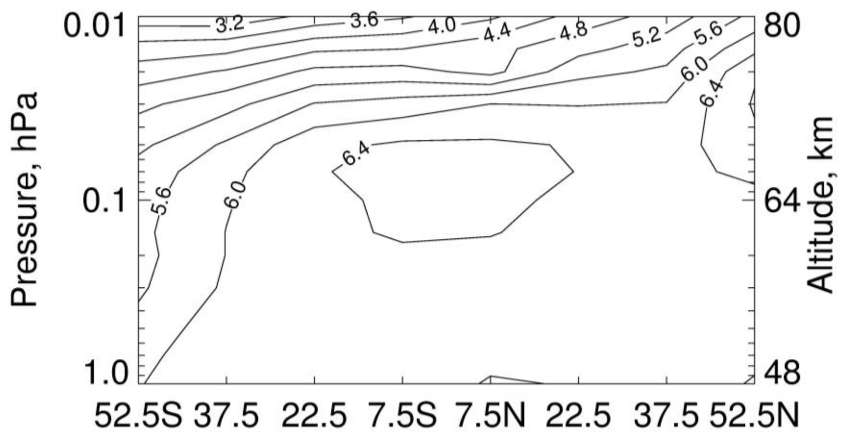

Figure 10—Climatological HALOE H_2O mixing ratio for (top) mid-January (day 15) and (bottom) mid-July (day 198). Contour increment is 0.4 ppmv.

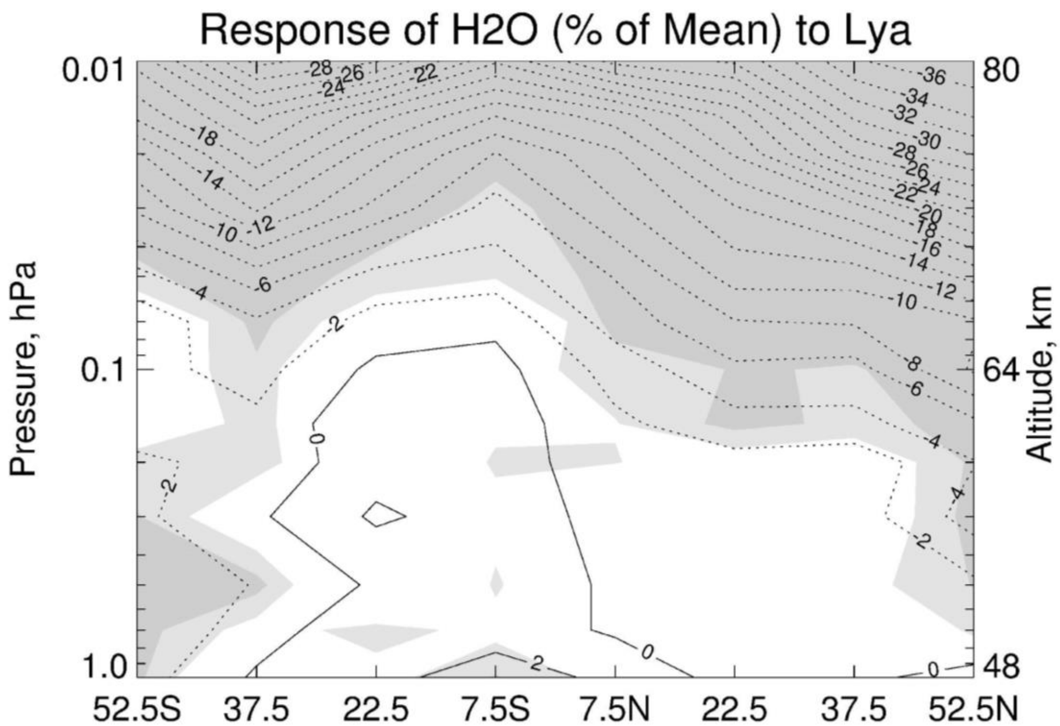

Figure 11—Distribution of the responses of H_2O to the maximum minus minimum Ly-α flux forcings (as % of the H_2O mixing ratios of Figure 1). Dashed contours are negative and contour interval is 2%. Confidence intervals (CI) are shaded as in Fig. 8.

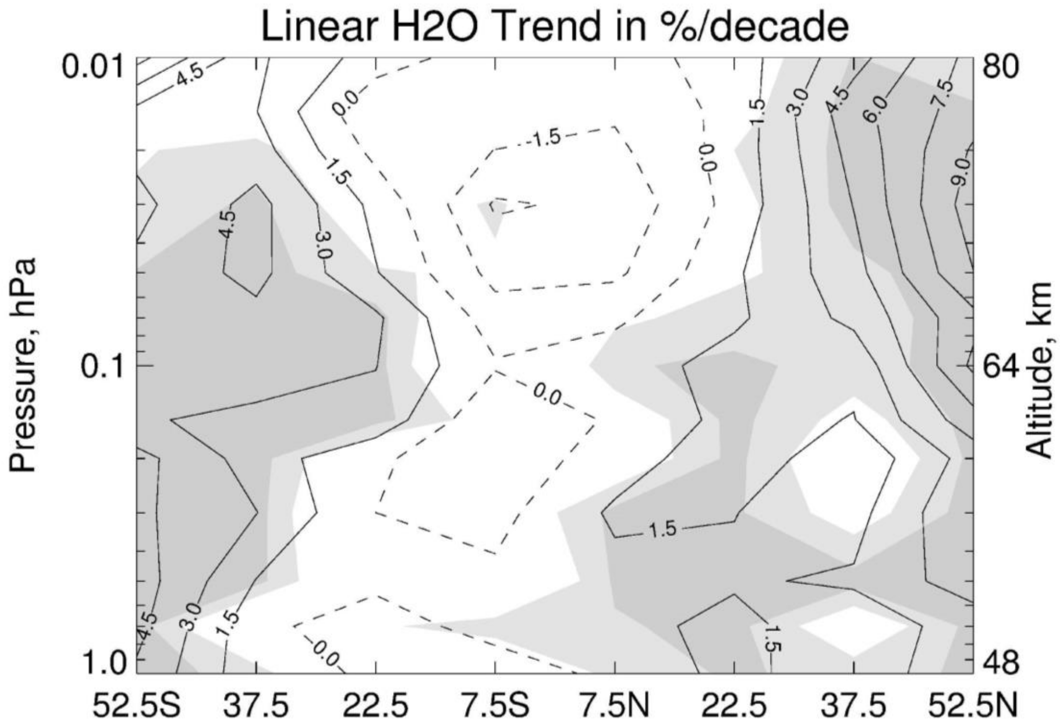

Figure 12—Distribution of the associated linear trend terms for H_2O from the MLR models (in %/decade as referenced to the Constant term). Solid contours are positive trends and contour interval is 1.5 %/decade. Shading denotes the CI, as defined for Fig. 8.

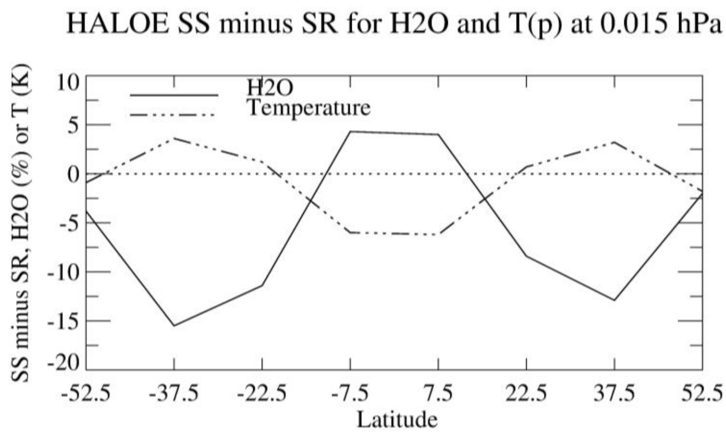

Figure 13—Average sunset (SS) minus sunrise (SR) differences versus latitude for H_2O and temperature at 0.015 hPa. H_2O and T differences are in (%) and K, respectively.

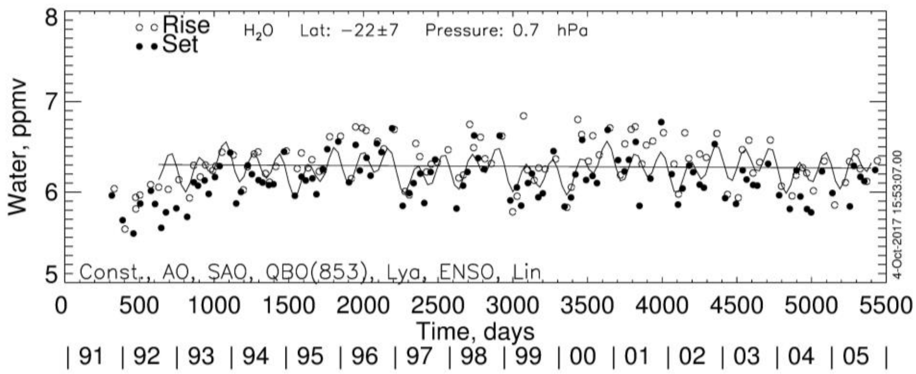

Figure 14—As in Figure 2, but for 22.5°S and 0.7 hPa.

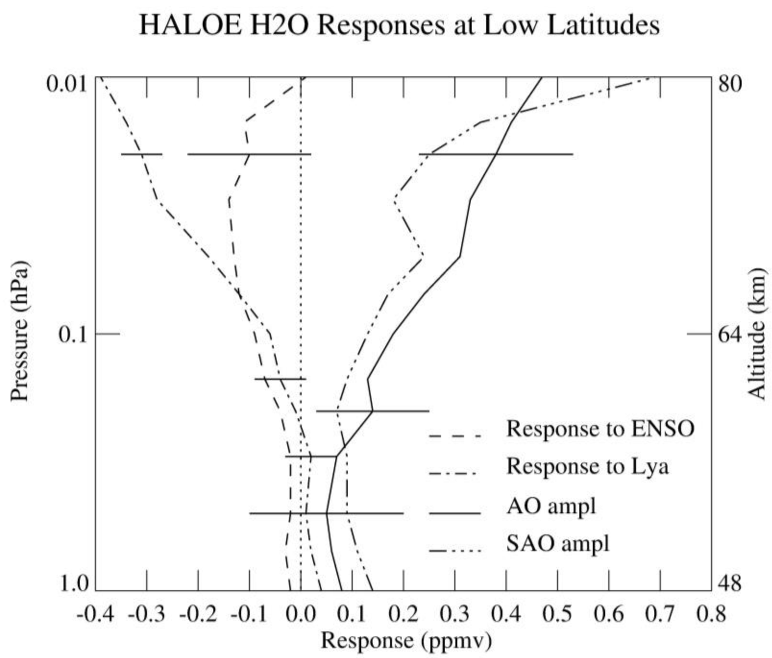

Figure 15—Average H_2O response profiles for the latitude region of 30°S to 30°N for comparison with those reported by *Nath et al.* [2017]. Horizontal bars are at selected levels for the AO, ENSO, and Lya terms, and they indicate ±1-σ values in each instance.